Polymer 115 (2017) 273–284

Contents lists available at ScienceDirect

Polymer

journal homepage: www.elsevier.com/locate/polymer

Interdiffusion of small molecules into a glassy polymer film via coarse-grained molecular dynamics simulations

Enqiang Lin [a], Xiaorong You [b], Robert M. Kriegel [b], Ronald D. Moffitt [c], Romesh C. Batra [a, *]

[a] Department of Biomedical Engineering and Mechanics, M//C 0219, Virginia Polytechnic Institute and State University, Blacksburg, VA 24061, USA
[b] Global Research, The Coca-Cola Company, 1 Coca-Cola Plaza, Atlanta, GA 30313, USA
[c] Global Engineering, The Coca-Cola Company, 1 Coca-Cola Plaza, Atlanta, GA 30313, USA

ARTICLE INFO

Article history:
Received 7 December 2016
Received in revised form
12 March 2017
Accepted 19 March 2017
Available online 21 March 2017

Keywords:
Diffusion
Polymer
Molecular dynamics
Coarse grained modeling

ABSTRACT

The interdiffusion of the C8, the C9 and the C10 aldehyde molecules into a glassy uncrosslinked polymer film composed of four components is studied by using coarse-grained (CG) molecular dynamics simulations. Effects of the aldehyde molecule size, water and temperature on the interdiffusion processes are probed. It is found that (i) the interdiffusion generally follows *the smaller-the faster* rule with the smallest C8 aldehydes diffusing fastest into the polymeric film, (ii) the water molecules significantly affect the adsorption and the initial interdiffusion of the aldehyde molecules onto/into the polymer film, (iii) the interdiffusions are strongly temperature dependent as the higher temperature enhances the initial dynamics of the aldehyde-polymer systems, (iv) the computed aldehydes diffusivities are highly concentration-dependent and increase with an increase in the concentration, and (v) the aldehydes density profiles scale as $t^{0.5}$ in the polymer-rich regions, and are well described by the Fickian diffusion with a constant diffusivity. Here t is the time of diffusion. Even though only relative values of the diffusivity coefficients can be predicted via the CG simulations, this work suggests that this approach is very useful in guiding the design and the selection of polymeric films with a tailored barrier property. Furthermore, it enables one to analyze small molecules-polymer interdiffusions into a polymeric film that is difficult to study experimentally but is of technological importance.

1. Introduction

The interdiffusion of small molecules into a polymeric matrix is an important factor in a variety of applications, such as food storage [1,2], membrane separation processes [3,4] and controlled drug release [5,6]. It is well accepted that this interdiffusion process depends not only on the molecular parameters of both small molecules and polymers (e.g., their chemical compositions, polarities, molecule sizes, shapes and concentrations), but also on their initial dynamics as reflected in the external environment conditions (e.g., the temperature and the aqueous environment that determine the mobility of small molecules and the relaxation rate of polymer segments). Due to the technological significance of small molecules-polymer interdiffusion, numerous efforts have been made to predict the underlying dynamic properties either experimentally [7–9], or theoretically [10–12] or computationally [13,14], for identifying mechanisms that could guide the development of new/modified polymeric materials with tailored transport properties. Among these efforts, molecular dynamics (MD) simulations are of particular interest since they enable one to follow time trajectories of all atoms in the system and provide detailed information of the motion of small molecules and their interactions with the polymers.

Early MD modeling of interdiffusion focused on the all-atom simulations of gases permeating into amorphous polymer melts and glasses [3,4,15–17]. These simulations revealed that the diffusion mechanism of small gas molecules is governed by a series of discrete jumps between small cavities in the polymer matrix. These all-atom simulations are based on the fact that the time scales for the motion of gas molecules are only weakly coupled with the segmental dynamics of polymers due to their small molecule sizes, which makes the occurrence of gas hopping mechanisms typically on the order of hundreds of picoseconds in molten polymers or tens of nanoseconds (and longer) in glassy polymers [18]. Thus, the gas diffusion constants can be quantitatively determined from the mean square displacements (MSDs) or the mass uptakes that are

* Corresponding author.
E-mail address: rbatra@vt.edu (R.C. Batra).

http://dx.doi.org/10.1016/j.polymer.2017.03.052
0032-3861/

Table 1
Components and their weight percentages in the polymeric film.

Component	Methyl acrylate	EAA	H_2O_2	Poly(ethyleneimine) solution 50% (w/v) in H_2O
Wt%	40	40	15	5

readily accessible with the standard atomic simulation approach.

With increasing demands of industrial applications, not only the diffusion of gases but the study of the diffusion of larger penetrant molecules such as solvents, oligomers, residual monomers, nanoparticles, plasticizers and other additives has also become very important [19–22]. Compared with the penetration of gases, the all-atom simulations of these larger molecule systems are much more computationally expensive. Most of the existing all-atom simulation examples have focused on analyzing the interdiffusion into the polymer melts that are far above the glass transition temperatures [20–23]. For example, Tsige and Grest [20] studied the interdiffusion of a spherical monomeric solvent into a homopolymer melt, and found that the process is dominated by the standard Fickian type diffusion with the weight gain scaled as $t^{1/2}$ (where t is the time of diffusion). Karlsson et al. [21] investigated the diffusion of limonene into molten polyethylene for 100 ns. The computed diffusivities and the activation energy were found to agree well with the corresponding experimental results. However, only a few papers describe the interdiffusion processes in glassy polymers [24,25]. The main difficulty for the all-atom simulations has been to conduct simulations for long enough times for the mean square displacements (MSDs) of the penetrant molecules to grow linearly in time or for the mass uptakes to reach the steady state. Alternative simulation approaches such as the united-atom [26,27], the coarse-grained [14,27,28] and the transition state methods [29,30] have been developed to overcome this difficulty. However, only the polymer systems composed of repeat units with a relatively simple structure, such as polyethylene (PE) [31], polypropylene (PP) [32,33], polyisobutylene (PIB) [34,35] and polyolefins [36] have been studied. A systematic investigation of more complex polymer systems that have multiple components is still lacking. The current work investigates the interdiffusion of three aldehyde molecules (C8, C9 and C10) into a commercial polymeric film composed of four different constituents, and is a first step in developing a polymer film with tailored barrier properties.

Besides the size of the penetrant molecules and the temperature, an important factor that can influence the interdiffusion is the presence of water molecules in the system. Owing to complex multiple interactions, the diffusion of penetrant molecules in aqueous solutions into the polymer matrixes may exhibit important differences in the interdiffusion of binary penetrator-polymer systems. This has been experimentally demonstrated for the transport of small organic molecules through polymer films. Aurélie et al. [37] studied the diffusions of four organic molecules into a PE film by three kinds of sorption experiments: a) solvent sorption by immersing films in pure penetrator compounds with liquid phase; b) vapor sorption by exposing films to saturated vapor phase, and c) solution sorption by immersing films in water solution containing penetrator compounds. Their results clearly showed that the presence of water could significantly modify the sorption of the penetrator molecules and reduce the corresponding diffusion coefficients. Aucejo et al. [38] studied the sorption of seven organic compounds in ethylene-vinyl alcohol copolymers, and found the water effect to be quite different for them. Since the interdiffusion in the aqueous environment is more "realistic", especially in the food industry, this study also probes the effect of water on the diffusion of three aldehyde molecules into the polymer film.

The aldehyde molecules (Octanal/C8, Nonanal/C9, Decanal/C10) are selected for their wide applications in the food industry as flavor/fragrance agents to obtain products with orange-like taste. During the storage of those products, the diffusion of aldehyde molecules into the protective polymeric lining often occurs, which then results in a loss of concentration balances in the food and affects the taste. The rates of their diffusion into the polymeric film play an important role in determining the concentration loss and the shelf life of the food. Thus, this work focuses on exploring the interdiffusion of the aldehyde-polymer systems via CG molecular dynamics simulation employing the MARTINI force field [39] and finding the corresponding diffusion constants to evaluate the barrier properties of the polymeric film. The effects of water, aldehyde molecule size and temperature are also probed.

The rest of the paper is organized as follows. In Section 2, we present details of the simulation models and the CG method. In Section 3, results for the interdiffusion in aldehyde-water-polymer ternary and aldehyde-polymer binary systems are presented. The evolution in time of the corresponding MSDs, density profiles and mass uptakes are analyzed. These results are briefly discussed in Section 4, and the main findings are summarized in Section 5.

2. Models and methods

The CG simulations of the aldehyde-polymer interdiffusions have been performed using a previously developed CG model [40]. In this model, the polymeric film is assumed to be made of four components: poly(methyl acrylate) (PMA) with 20 repeating units (n = 20), poly(ethylene-*co*-acrylic acid) (EAA) with 3 repeating monomers (n = 3) of 14 mers ethylene (x = 14) and 1 mer acrylic (y = 1), linear poly(ethyleneimine) (LPEI) with 10 repeating units (n = 10) and branched poly(ethyleneimine) (BPEI) polymer with only 1 repeating unit. The film is formed by mixing desired % weights, listed in Table 1, of methyl acrylate, EAA, hydrogen peroxide (H_2O_2) and poly(ethyleneimine) solution (50% (w/v) in H_2O). Figs. 1 and 2 show chemical structures of the four polymer components and their CG mappings. In these CG models (Fig. 2), on the average, two or three heavy atoms (non-hydrogen) are mapped into one CG bead. With this mapping strategy, the polymers' structural characteristics are well kept. The PMA and the EAA polymers are described by Na-SC2 and SC2-SP3 beads in the MARTINI force field, which are defined on the backbone and the

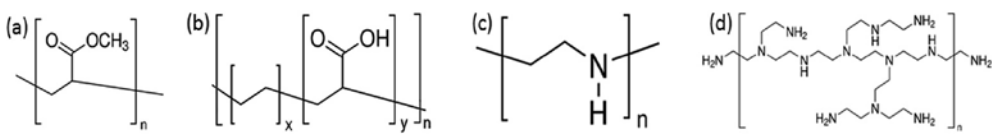

Fig. 1. Chemical structures of (a) PMA; (b) EAA; (c) LPEI, and (d) BPEI.

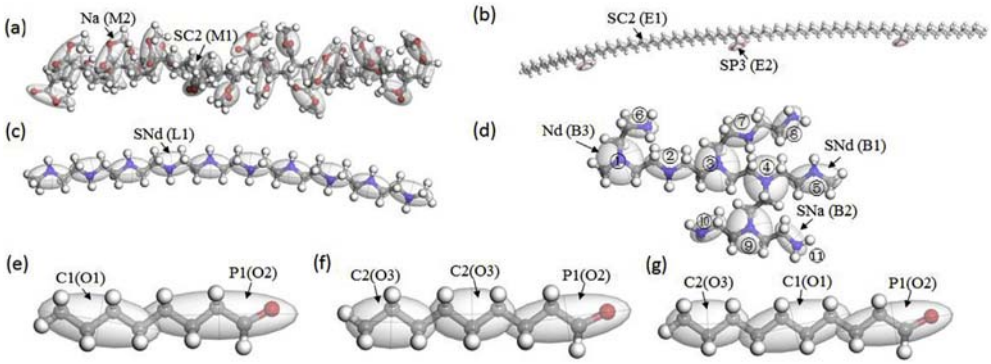

Fig. 2. Coarse-grained mappings of (a) PMA, (b) EAA, (c) LPEI polymer, (d) BPEI polymer, (e) C8 molecule, (f) C9 molecule, and (g) C10 molecule. The labels indicate the CG beads used in the MARTINI force field.

side atoms. Their masses are set equal to 72—26 and 26—45 amu. The LPEI and the BPEI polymers are represented by SNd, Nd and SNa beads according to the amino groups in their structures. The corresponding masses are 45, 56 and 45 amu. The three aldehyde molecules are described by C1-P1, C2-C2-P1 and C2-C1-P1 beads with masses equal to 72-72, 45-45-72 and 45-60-72 amu. For the interactions among CG beads, distributions of distances and angles from the atomistic simulations are used to parametrize the bonded interactions. The non-bonded interactions are characterized by the following conventions in the MARTNI force field to reproduce the mass density and the radius of gyration of the polymer chains from the atomistic simulations. These CG parameterization results are given in Appendix A. They have been verified to well describe the diffusion of the aldehyde molecules into the polymer film composed of above four components [40].

The above given CG models for each component are used to prepare the polymeric film. Based on the weight proportion listed in Table 1, 20 CG PMA chains, 87 CG EAA chains, 5 CG LPEI chains and 5 CG BPEI chains are chosen to represent the polymeric film. Due to the complex polymerization reactions involved in preparing the film, it is very challenging to construct a CG model that accurately describes the connected polymeric film system. Thus, in the current study, the simulated film is prepared by directly mixing the four components without modeling crosslinking. By investigating this uncured film, deep insights into the interdiffusion of the aldehyde molecules into this polymeric film can still be gained. Note that the cross-linking algorithms to construct CG models with complex network structures are available in the literature if the curing reaction mechanisms are known [41].

Given the initial mixing system, the CG polymeric film is prepared as follows through the densification and relaxation processes. All simulations of these processes are carried out using the MD package LAMMPS [42]. First, we add two impenetrable walls on either side of the system in the z-direction to compress the film at 300 K. Then, the system is annealed to relax the compressed film and release the internal stresses while keeping the two walls fixed. Subsequently, the upper wall is removed and the system is further relaxed to minimize the surface energy. The thus prepared film measures 12.53 nm $\times$ 12.30 nm $\times$ 11.56 nm and consists of 28,920 beads with a mass density of 0.958 gcm^{-3} in its central region at 300 K. To perform the interdiffusion simulations, a 12.53 nm $\times$ 12.30 nm $\times$ 11.60 nm box containing 2000 CG aldehyde molecules and 10,000 P4 water beads is prepared and assembled on top of the film. A rigid wall is again added on top of the water layer to prevent evaporation of water molecules in subsequent simulations. The walls' interactions with the aldehyde-water-polymer systems are set to be weak enough to minimize their influence on the interdiffusion dynamics. The assembled interdiffusion models are then equilibrated first in the NPT ensemble to relax the configurations, and then the simulations are performed in the NVT ensemble to realize the interdiffusion. During simulations, periodic boundary conditions are applied in both the x- and the y-directions in the final models. The time step is set equal to 10 fs. The one-dimensional (1D) binning analysis [43,44] with a thickness of 4 Å in the z-direction is performed to monitor evolutions of the mass density profiles as a result of the interdiffusion. The MSDs of the aldehyde molecules, the water molecules and the polymer chains are also monitored for analyzing their dynamic behaviors.

3. Results

3.1. Interdiffusion of aldehyde-H_2O-polymer ternary systems

The first objective of this work is to investigate effects of water on the interdiffusion of the aldehyde molecules into the polymer film since the occurrence of interdiffsuion in aqueous environment is commonly seen in many industrial applications (e.g., the canned foods). Fig. 3 shows the initial setup and snapshots of the microstructural evolution for the three aldehyde-H_2O-polymer systems. In Fig. 3, the aldehyde molecules are described by green and red beads (they represent the C- and the P-type beads in Fig. 2e—g, respectively), the water molecules by white beads, while the EAA and the PMA polymer chains are represented, respectively, by purple and brown beads. From these results of the microstructure evolution, the following three phenomena can be observed: a) the phase separation between the aldehyde and the water molecules in which the aldehyde molecules gradually accumulate to form clusters and then layers (Fig. 3b, f and g); b) the adsorption of the aldehyde molecules onto the polymer film surface, and c) the interdiffusion between the adsorbed aldehyde layers and the polymer chains (Fig. 3c, g and k).

The phase separation phenomenon can be understood from the hydrophilic (P1) and the hydrophobic (C1 or C2) beads that make up the CG aldehyde molecules in the current simulations. When the aldehyde molecules interact with the water molecules (P4 beads), the hydrophilic P1 beads tend to bind with the water molecules while the hydrophobic C-type beads tend to repel from the water molecules. As a result of the energy minimization, the aldehyde molecules accumulate to form a cluster/layer structure with the hydrophilic P1 beads pointing to the water molecules. Therefore, in Fig. 3c, f and 3i, relatively more red P1 beads are observed in the phase interfaces formed on top of the polymer film and the outer surface of the water layer. This mechanism is quite similar to the

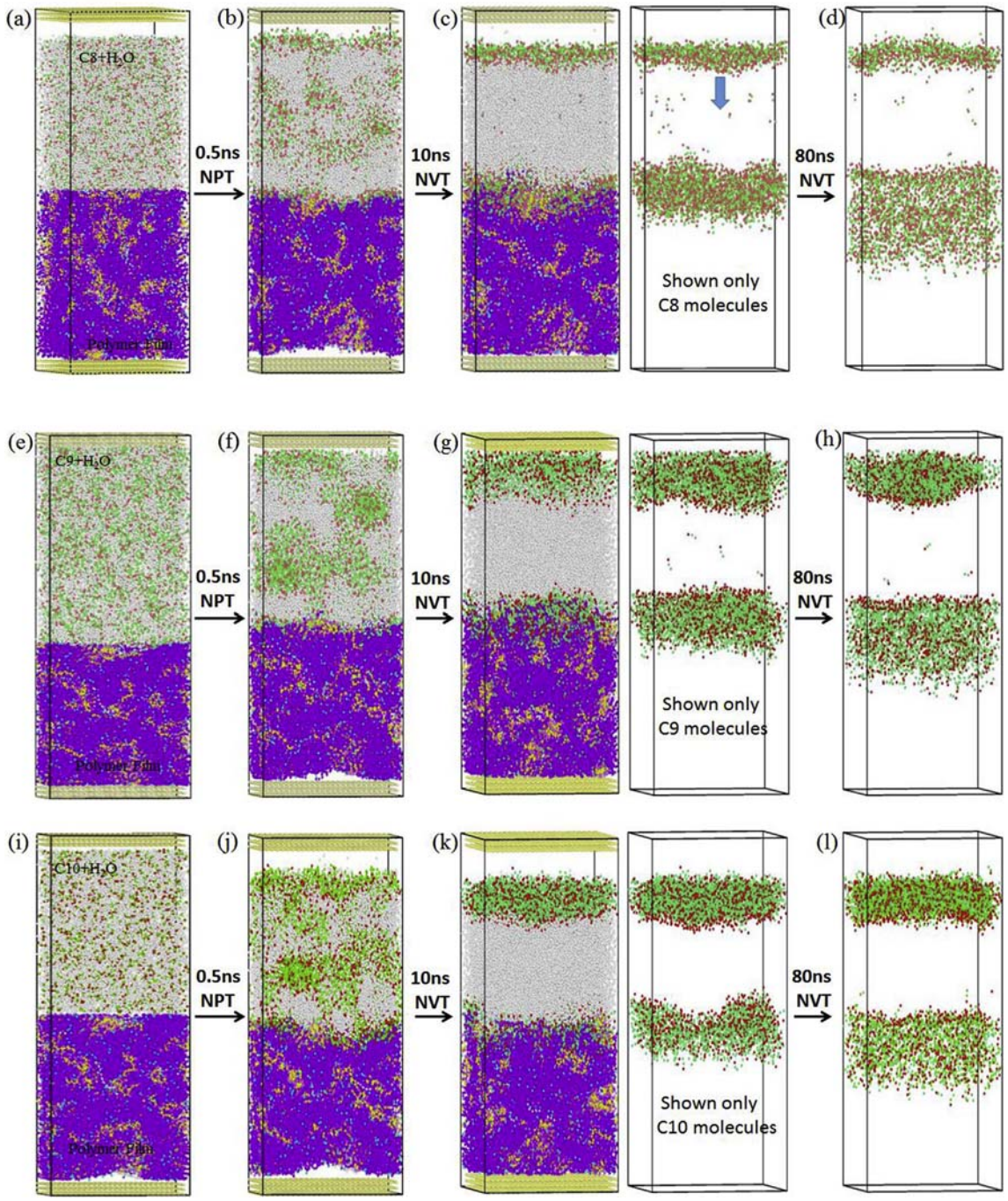

Fig. 3. Diffusion of (a)–(d) C8 molecules, (e)–(h) C9 molecules and (i)–(l) C10 molecules into the polymer matrix at T = 300 K. White beads represent water molecules; Yellow beads at the top and the bottom are the two rigid walls; Purple and Brown beads represent the EAA and the PMA chains, respectively; Red and Green beads represent either the C8, or the C9 or the C10 molecules. The polymers and H_2O in Fig. 3c, g and 3k are not shown for clearly viewing the diffusion of the C8, the C9 and the C10 molecules. The arrow in Fig. 3c indicates the adsorption of C8 molecules at the water free surface onto the polymer surface. (For interpretation of the references to color in this figure legend, the reader is referred to the web version of this article.)

formation of a bilayer structure for the lipid molecules in water. The simulated phase separation phenomenon is consistent with the known results that the C8, the C9 and the C10 aldehyde molecules, with respective solubilities of 560, 96 and 15.6 mg/L [45], are immiscible in water at room temperature. Since the solubility of the aldehyde molecules decreases as the chain length increases, the hydrophobic effect thus becomes more significant, especially for the C10 molecules. Therefore, we note that in Fig. 3c, f and 3i the number of dissolved aldehyde molecules decrease in the order, C8 > C9 > C10. The agreement of these observations with the known results implies that the developed CG models with the interaction parameters well capture main features of the aldehyde-water interactions.

During phase separation, the aldehyde molecules are observed to gradually absorb onto the polymer surface, forming a thin covering layer of aldehyde molecules without water (Fig. 3c, f and 3g). The adsorption of aldehyde molecules is spontaneous which is due to the hydrophobic effect and the van der Waals interactions.

Since the van der Waals interactions have a cutoff distance of 12 Å in current simulations, thus only a portion of the aldehyde clusters that are within the cutoff distance are absorbed onto the polymer surface. Therefore, along with the adsorption, we also observe the accumulation of the aldehyde molecules at the free surface of the water layer. Thus a "sandwich" structure is finally formed in these ternary systems with the polymer film in the substrate, a thin aldehyde layer in the middle and a water layer on the top. In these sandwich structures, no mass transport is observed between the two aldehyde layers for the C9 and C10 molecules. However, due to its higher solubility in water with weaker hydrophobic effect, the C8 molecules at the water free surface are found to slowly adsorb onto the polymer surface, as shown by the arrow in Fig. 3c.

The interdiffusion between the aldehyde layer and the polymer substrate occurs immediately after the formation of the sandwich structure that is driven by the chemical miscibility and the concentration gradient. Unlike the hopping mechanism observed in the penetration of small gases, the diffusion of much larger aldehyde molecules in current simulations is found to be dominated by the segmental dynamics of polymer chains. That is, the aldehyde molecules do not directly penetrate into the dense film interior unless the polymer segments diffuse first into the aldehyde-rich region and then open the free spaces for them. During the interdiffusion, only a few water molecules are observed to penetrate into the polymer film even after the whole aldehyde layer is dissolved by the polymer matrix. This is consistent with the water resistance nature of EAA polymers that makes 40%wt of the film confirming again the capability of the developed CG models for the analysis of aldehyde-water-polymer interdiffusion. From the barrier perspective, the presence of water plays an important role in hindering the motion of polymer chains at the interface region. It reduces the diffusion rate of the aldehyde molecules from the interface into the film interior. However, this effect is inferred to be negligible as the aldehyde molecules diffuse deep into the film.

The overall dynamic behaviors of the aldehyde and the water molecules are also monitored during the simulations. In Fig. 4 we have plotted the time-dependent averaged MSDs and the self-diffusion coefficients of the aldehyde and the water molecules for the three simulated systems. As expected the MSDs of the water molecules in the three systems are quite similar to each other since they share the same diffusion mechanisms with the formation of the water layer after phase separation (see Fig. 3). While the MSDs of the aldehyde molecules show an obvious size-dependent characteristic, it decreases as the molecule size increases in the order C8 > C9 > C10. Given the MSDs, the self-diffusion coefficients can be obtained by using the Einstein relation $D_s(t) = \lim_{t\to\infty} MSDs/6t$ (where t is time) and results are shown in Fig. 4b. Three stages of the aldehyde and the water molecules diffusion can be observed in Fig. 4b. The first stage displays a significant reduction in the self-diffusion coefficients for the two molecules which is related to their phase separation and adsorption processes in the time interval [0,10] ns (as shown in Fig. 3c, g and 3k). The second stage generally shows an increase of the self-diffusion coefficients for the two molecules which is due to the initial interdiffusion between the adsorbed aldehyde molecules and the polymer film in the time interval [10,40] ns. In the third stage the self-diffusion coefficients reach a plateau for the two molecules indicating the steady state diffusion. This is not surprising and is related to the steady interdiffusion between the aldehyde molecules and the polymer film (see Fig. 3d h and l). This confirms the previous inference that the water effect is negligible as the aldehyde molecules diffuse deep enough into the film. In this third stage, the self-diffusion coefficients of water molecules are calculated to equal 2.217×10^{-5}, 2.203×10^{-5} and $2.233 \times 10^{-5} cm^2 s^{-1}$, respectively. These results agree well with the computed self-diffusion rate of $2.0 \times 10^{-5} cm^2 s^{-1}$ for the pure CG water particles and the experimental diffusion constant of $2.3 \times 10^{-5} cm^2 s^{-1}$ at 300 K [46]. Meanwhile, the self-diffusion coefficients of the aldehyde molecules are calculated to equal 1.983×10^{-5}, 1.348×10^{-5} and $0.718 \times 10^{-5} cm^2 s^{-1}$ for the three cases, i.e., the self-diffusion coefficients decrease with an increase in the molecule chain length. Here, it should be noted that the above calculated self-diffusion coefficients of the aldehyde molecules can only be treated as reference values for illustrating the size effect. They are not the absolute self-diffusion constants for the diffusion of aldehyde molecules into water or into the polymer film, because their behaviors in the system are confined in the non-periodic z-direction, which deviates from the isotropic diffusion behavior. However, for water molecules, the diffusion coefficient is derived from the relatively thick water layers (~85 Å) formed after the phase separation (Fig. 3c, g and 3k). Since the majority of water molecules in the central region of the layers still obey the isotropic diffusion assumption, thus, the calculated self-diffusion coefficient is found to be comparable with the experimental result.

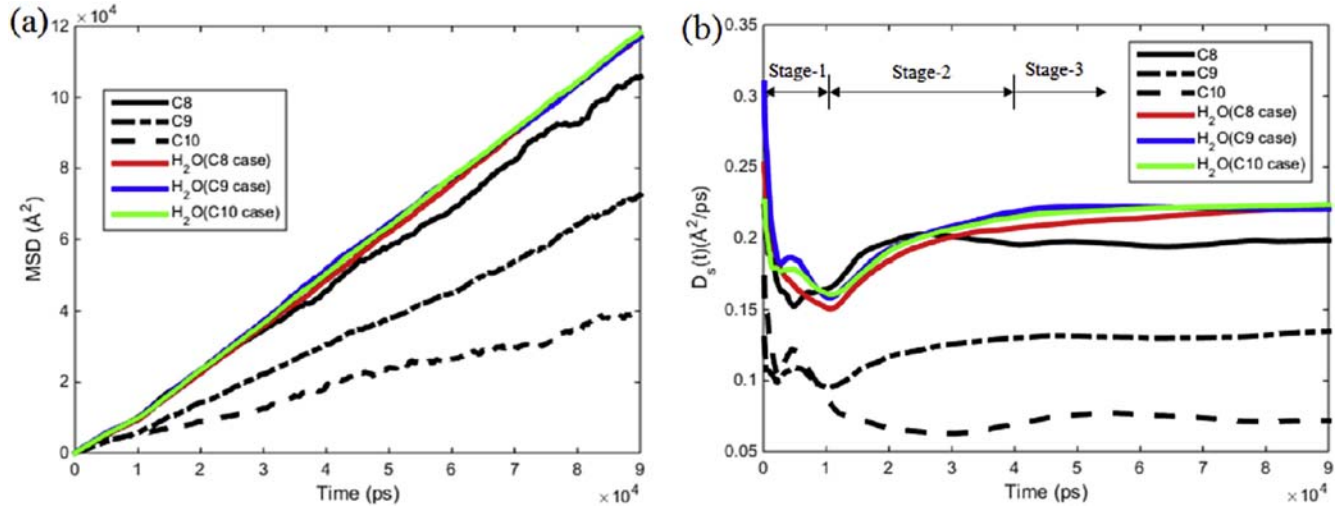

Fig. 4. Time histories of the (a) averaged MSDs and (b) the self-diffusion coefficients of the aldehyde and the water molecules for the three simulated systems at T = 300 K.

3.2. Interdiffusion of aldehyde-polymer binary systems

Another objective of this work is to measure the diffusivity constants to evaluate the barrier properties of the polymer film. The simulations of the ternary systems have revealed that they may not be suitable for investigating the long-time interdiffusion behaviors due to the limited number of aldehyde molecules absorbed on the film surface. Therefore, the aldehyde-polymer binary systems (without water) are employed for this study. The use of binary models is based on the following observations: a) the interdiffusion only occurs between the adsorbed aldehyde layer and the polymer film after the formation of a sandwich structure; b) the water molecules are seldom found to diffuse into the film due to the water resistant nature of the polymeric film, and c) the water effects on the long-time aldehyde-polymer interdiffusion are negligible. Therefore, the binary systems can be regarded as equivalent to the equilibrated ternary systems that have a thick aldehyde layer at the polymer surface in their sandwich structures.

Fig. 5 shows the initial setups for the three binary aldehyde-polymer systems at 300 K and evolutions of their microstructures during the interdiffusion. As shown in snapshots of the microstructure (Fig. 5a, e and i), the contact interfaces of all three binary systems are relatively smooth at the beginning of simulations (t = 0 ns). The corresponding arithmetic averages of the roughness R_a (calculated based on the polymer film surface) are 5.68 Å, 8.04 Å and 6.63 Å for the C8, the C9 and the C10 systems, respectively. They swell at different rates as the interdiffusion proceeds. The C8 case is the most pronounced one since the polymer chains are found to diffuse most among the three cases into the aldehyde layer (indicated by the dash lines in Fig. 5). The C9 molecules come second and the C10 molecules the last. All three cases show the same asymmetric interdiffusion characteristics, i.e., the polymer chains diffuse much deeper into the aldehyde layer than the aldehyde molecules into the polymeric film. This asymmetric interdiffusion is not surprising since the liquid nature of the aldehyde molecules with high mobility promotes the diffusion of polymer chains into the aldehyde layer. The mobility of the aldehyde molecules depends on the size of their molecules -the smaller molecules generally have higher mobility. Thus, as expected the polymer chains diffuse deepest into the C8 layer as shown in Fig. 5c.

The time-dependent mass density profiles for the two components in the binary systems, $\rho_{polymer}$ and $\rho_{aldehyde}$, which are obtained from the 1D binning analysis, are also plotted in Fig. 5 to quantify the interdiffusion. The density profiles for the three aldehyde-polymer systems have similar shapes. They differ in their evolution rates. From the depth of penetration, we conclude that the C8 aldehyde diffuses deeper than the C9 and the C10 aldehydes indicating a higher diffusivity. Asymmetric interdiffusions can also be seen in these density profiles. On the polymer-rich side of the interfaces where the relatively slow polymer relaxation dominates the interdiffusion, the aldehyde density profiles evolve gradually into a convex shape as the simulation proceeds implying the accumulation of the aldehyde molecules and the formation of the diffusion fronts at the interfaces. Scaling the density profiles with $t^{0.5}$, both the aldehyde and the polymer density profiles in these polymer-rich regions collapse into a single master curve as shown in Fig. 6 thereby indicating the Fickian diffusion behaviors [24]. However, on the aldehyde-rich side where the relatively fast aldehyde mobility dominates the interdiffusion, both the aldehyde and the polymer density profiles become rough and no longer scale with $t^{0.5}$. This lack of $t^{0.5}$ scaling of the mass density profiles was also observed by Pierce et al. who simulated the interdiffusion of short chain oligomers into an entangled polymer film [25] which is attributed to the slow polymer swelling effect. According to the theoretical analysis of Kubo and Nose [47], the single EAA and PMA polymer chain dynamics in the aldehyde-rich region would generally follow the Zimm-type diffusion model due to the strong hydrodynamic interactions between the long polymer chain and the short chain of the aldehyde solution. Their behaviors in the aldehyde solution are more like a rigid sphere in translational diffusion as a result of the hydrodynamic interactions, which thus may also contribute to the lack of $t^{0.5}$ scaling of the mass density profiles in the aldehyde-rich region.

Two diffusion models have been used to extract the diffusivity from the mass density profiles. In the first model, the diffusivity is assumed to be independent of the aldehyde mass density. The Fickian diffusion function (Eq. (1)) thus is used to fit the $t^{0.5}$ scaled density profiles (Fig. 6) to find the diffusivity constant, D_0:

$$\rho(z,t) = \rho_0\left(1 - \mathrm{erf}\left(\frac{z}{2\sqrt{(D_0 t)}}\right)\right) \tag{1}$$

Here ρ_0 is the equilibrium aldehyde concentration in the polymer and erf is the error function. This simple function is used based on the demonstrated Fickian-type diffusion in the polymer-rich regions and its wide application to fit the experimental data [20]. Two sets of scaled density data are used in the fitting process: the scaled densities in only the polymer-rich region (Fitting-1) and the scaled densities in the entire interdiffusion region (Fitting-2). The fitting results are shown in Fig. 6 and summarized in Table 2. The corresponding diffusivity constants are: $D_0^{C8} = 4.76 \times 10^{-7} cm^2 s^{-1}$, $D_0^{C9} = 3.581 \times 10^{-7} cm^2 s^{-1}$ and $D_0^{C10} = 2.925 \times 10^{-7} cm^2 s^{-1}$ for fitting-1; $D_0^{C8} = 15.40 \times 10^{-7} cm^2 s^{-1}$, $D_0^{C9} = 10.94 \times 10^{-7} cm^2 s^{-1}$ and $D_0^{C10} = 13.33 \times 10^{-7} cm^2 s^{-1}$ for fitting-2. Due to the non-Fickian kinetics in the aldehyde-rich regions, the diffusivity constants extracted from fitting-2 data sets are generally 3- to 5-time higher than those obtained from fitting-1 data sets. However, all these diffusivity values ($D_{C8} > D_{C9} > D_{C10}$) agree with the size-dependent mobility of the aldehyde molecules reported above.

In the second model, Fick's second law (Eq. (2)) is used in conjunction with the density profiles to measure the density/concentration dependent diffusivity [25], D(ρ):

$$\frac{\partial \rho(z,t)}{\partial t} = \frac{\partial}{\partial z}\left[D(\rho(z,t))\frac{\partial \rho(z,t)}{\partial z}\right] \tag{2}$$

In the polymer-rich regions, D(ρ) can be calculated by integrating Eq. (2) by using the Boltzmann transformation ($\eta = zt^{0.5}$):

$$\mathrm{D}(\rho) = -\frac{1}{2}\left(\frac{d\rho'}{d\eta}\Big|_{\eta(\rho)}\right)^{-1}\int_{\eta_0}^{\eta}\eta'\frac{d\rho}{d\eta'}d\eta' \tag{3}$$

Here η_0 is the scaled position where the aldehyde density becomes zero. To apply Eq. (3), the average aldehyde density profiles ρ(η) in the polymer-rich regions are first fitted by a 9-degree polynomial function. Then, differentials of this polynomial function ($\eta d\rho/d\eta$) are integrated up to the target density to calculate the corresponding diffusivity. This procedure is repeated for different aldehyde density and the final D(ρ) calculated for the three aldehyde systems are plotted in Fig. 7.

In general, the behaviors of D(ρ) are quite similar for the three aldehyde systems studied. For each one of them D(ρ) increases with an increase in the aldehyde concentration. Within the investigated density range, the diffusivities of the C9 and the C10 aldehydes are close to each other but less than the diffusivity of the C8 aldehydes. These observations agree with the microstructure evolution results shown in Fig. 5. Two types of D(ρ) behaviors can be seen in Fig. 7. At the low density range (<0.1), D(ρ) for all three systems increases dramatically with the increase in the

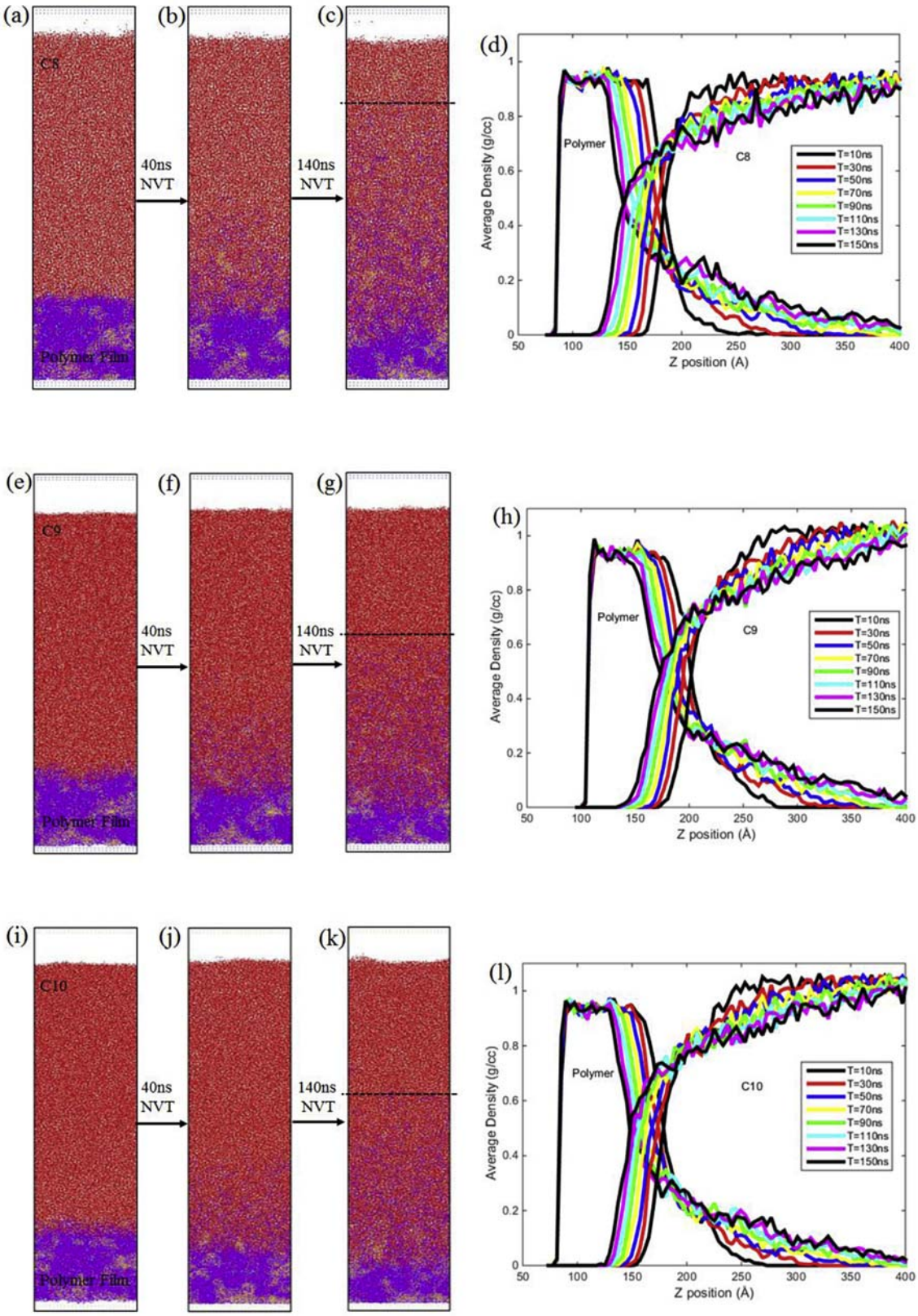

Fig. 5. Microstructure and density profile evolutions of the aldehyde molecules and the polymers interdiffusion at T = 300 K and t = 0 ns, 40 ns, 140 ns: (a)–(d) the C8 molecule; (e)–(h) the C9 molecule, and (i)–(l) the C10 molecule. The red color represents the aldehyde molecules, and the purple and the brown colors stand for the EAA and the PMA polymer chains, respectively. The black dash lines indicate the diffusion depth of the polymer chains into the aldehyde-rich region. (For interpretation of the references to color in this figure legend, the reader is referred to the web version of this article.)

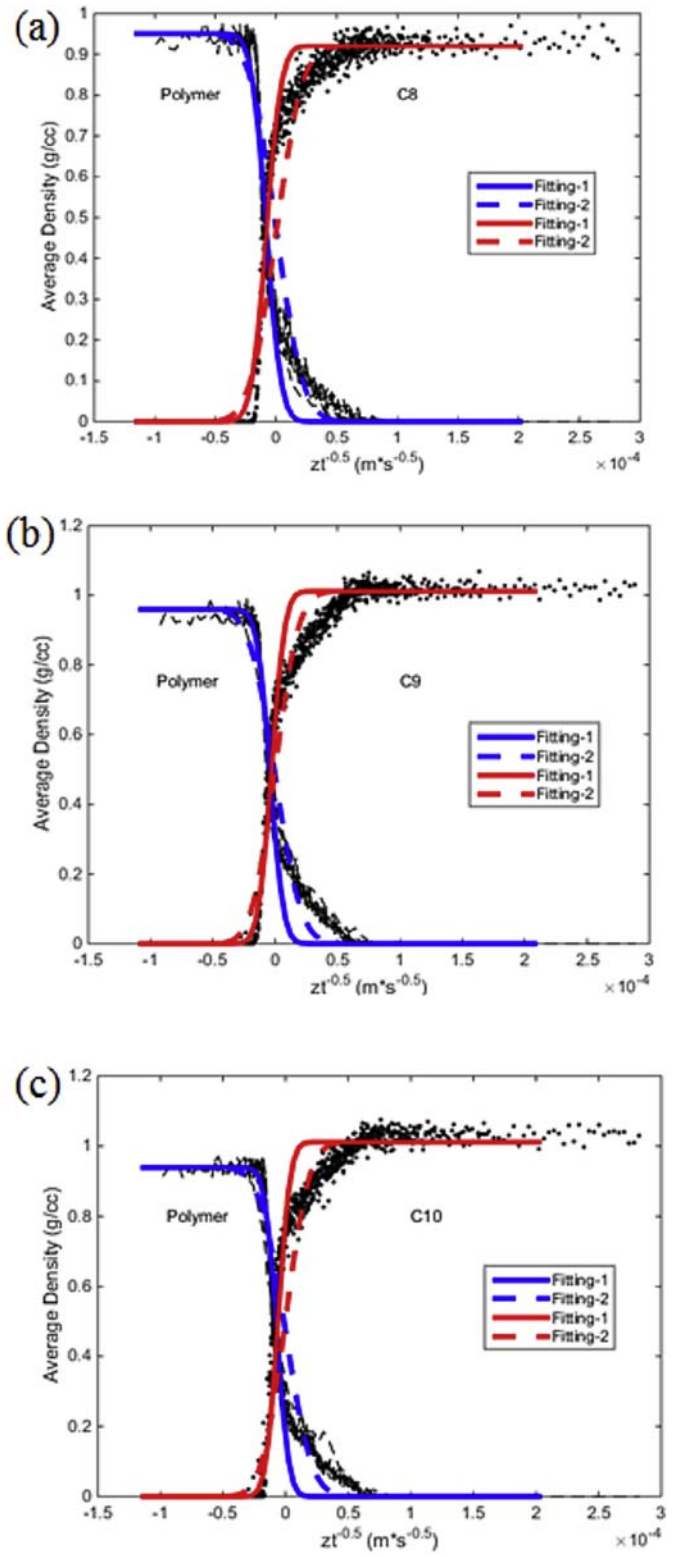

Fig. 6. Density profiles for the three aldehyde-polymer systems scaled with $zt^{-1/2}$ at T = 300 K: (a) C8-polymer system; (b) C9-polymer system, and (c) C10-polymer system. The solid and the dashed lines are curves fitted by using methods 1 and 2, respectively.

concentration which may be related to the large free-spaces available in the polymer interface to accommodate the aldehyde molecules. At the higher density (the saturation of free-spaces at the interface), D(ρ) increases exponentially with an increase in the concentration. This exponential increase is often observed for the interdiffusion of monomers with glassy polymer films [24,25], and can be approximated by the exponential function $D(\rho) = D_0' \exp(\alpha\rho)$ (where D_0' and α are constants) as shown in Fig. 7. The approximate values of D_0' for the three aldehyde systems are $D_0^{C8} = 3.023 \times 10^{-7} cm^2 s^{-1}$ (with $\alpha = 1.637$), $D_0^{C9} = 2.593 \times 10^{-7} cm^2 s^{-1}$ (with $\alpha = 1.666$) and $D_0^{C10} = 2.544 \times 10^{-7} cm^2 s^{-1}$ (with $\alpha = 1.664$), respectively. These values compare well with those obtained from the simple Fickian diffusion model (Eq. (1)). Thus as a first approximation, treating D(ρ) as a constant is a reasonable assumption for studying the interdiffusion of the aldehyde-polymer in the polymer-rich region.

The computed mass uptakes of the aldehyde molecules by the polymer film for the three systems are shown as a function of both $t^{0.5}$ and t in Fig. 8. The mass uptakes are measured by counting the number of aldehyde molecules that diffuse below the initial (at t = 0) aldehyde-polymer interface thereby excluding the swelling effect of the polymer film. This simple fixed interface position is employed due to the ambiguous definition of the swelling interface during the simulation. Therefore, it should be noted that the counted mass uptakes are always underestimated and the situation becomes worse as the interface gradually moves upwards. From results depicted in Fig. 8, it is seen that the weight gain increases linearly with t rather than with $t^{0.5}$ for the three aldehydes. It deviates significantly from the Fickian-type diffusion observed in the density profiles in Fig. 6. The underestimated aldehyde numbers and the enhanced limited-effect of the time-independent viscoelastic relaxation of the polymer chains on the maximum aldehyde flux at the diffusion front as it propagates ahead may be two major factors for the deviation. Indeed, we see in Fig. 5 that a convex upwards density profile shape is gradually established as the simulation proceeds, implying that the mass uptakes become more and more limited to the Case II aldehyde flux at the diffusion front. By comparing slopes of the mass uptake curves, we find that the C8 aldehydes exhibit the fastest diffusion rate and the diffusion rates of the C9 and the C10 aldehydes are close to each other but less than that of the C8 molecules. These observations again are well consistent with the above microstructure and the fitted density profile results shown in Figs. 5–7, and can be attributed to the CG molecule sizes. The C8 molecules in the current CG models are represented by C1-P1 beads, while the C9 and C10 molecules are described by C2-C2-P1 and C1-C2-P1 beads in the MARTINI force field. Since the majority of non-bonded interactions between beads in the polymer film and the C1 bead are the same as those for the C2 bead (see Table A2), the polymer film treats the C9 and the C10 aldehydes as almost the same molecules, which then results in the close diffusivities and mass uptakes of the C9 and the C10 aldehydes shown, respectively, in Figs. 7 and 8.

3.3. Temperature effect

The initial dynamics of an aldehyde-polymer system as reflected in the temperature being lower/higher than the glass transition temperature, Tg, significantly affects their interdiffusions. For the polymer film without cross-linking being studied, the Tg is around 315 K and is calculated from the density-temperature relation by relaxing the CG polymer system from 500 K to 200 K at the rate of 0.06 K/ns as shown in Fig. 9. It is expected that the Tg will increase when the cross-linking or curing mechanism is considered for the polymeric film [48]. The temperature range, 277 K–313 K, that is below the calculated Tg thus is used to study the temperature effect. The results are summarized in Table 2 and plotted in Fig. 10 with the diffusivity constants obtained by fitting the simple Fickian diffusion model (Eq. (1)) to the corresponding density profiles

Table 2
Extracted diffusivity constants from the $t^{0.5}$ scaled density profiles.

Temperature (K)	D_{C8} ($\times 10^{-7} cm^2 s^{-1}$)		D_{C9} ($\times 10^{-7} cm^2 s^{-1}$)		D_{C10} ($\times 10^{-7} cm^2 s^{-1}$)	
	Fitting-1	Fitting-2	Fitting-1	Fitting-2	Fitting-1	Fitting-2
277	1.24	4.944	0.668	2.544	0.554	2.515
300	4.76	15.40	3.581	10.94	2.925	13.33
313	9.98	28.07	7.208	19.17	5.434	21.41

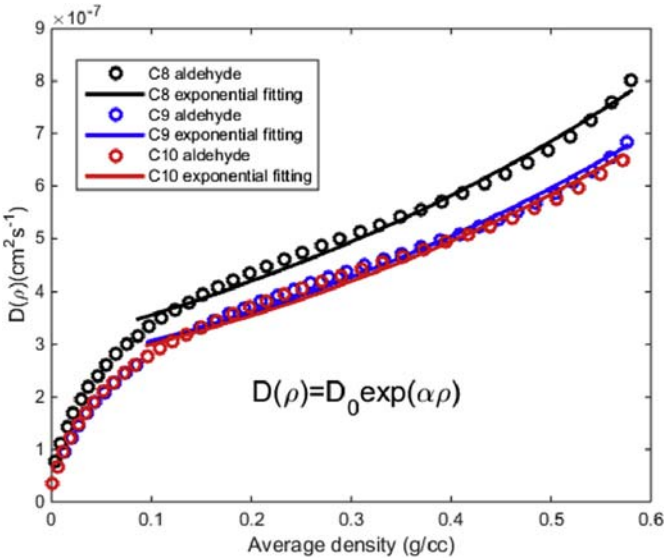

Fig. 7. Concentration-dependent diffusivities D(ρ) as a function of the average density for the three aldehydes studied. The solid lines are exponential fits to the computed values.

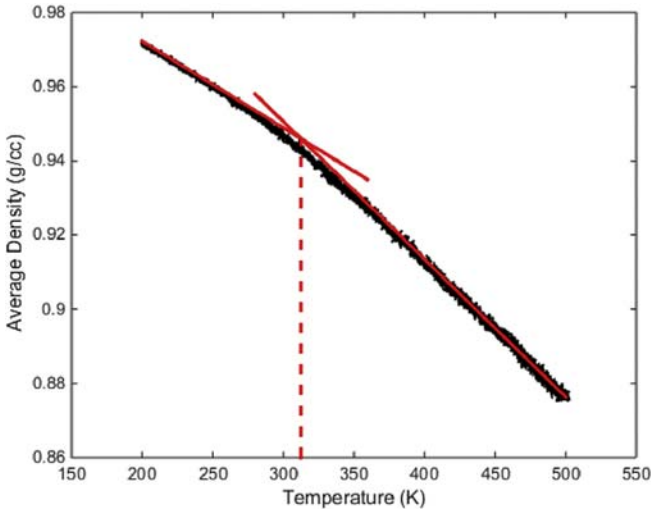

Fig. 9. Density versus temperature relationship for the polymer film system.

discussed in Section 3.2.

As seen in Fig. 10, the diffusivity constants of the three aldehyde molecules increase with an increase in the temperature. However, the increase in the C8 diffusivity is more pronounced at high temperatures implying a higher temperature sensitivity of the C8 aldehydes than that of the C9 and the C10 aldehydes. This higher temperature sensitivity can be attributed to the smaller size and the higher mobility of the C8 aldehydes that facilitate their penetration into the film when the polymer film is being relaxed. An examination of the density profiles (not shown) reveals that within the investigated range of the temperature, it does not alter the interdiffusion mechanisms between the aldehydes and the polymeric film, which is approximately the Fickian-type diffusion in the polymer-rich region and the non-Fickian diffusion in the aldehyde-rich region as stated in Section 3.2. However, as the temperature is further reduced and the cross-linking in the film is considered, a Case II diffusion can be expected in the polymer-rich region [20].

4. Discussion

The nearly Fickian-type diffusion in the polymer-rich region rather than the expected Case II diffusion in glassy polymers is observed in current simulations. This Fickian behavior might be related to the short EAA (n = 3) and PMA (n = 20) chains and the uncured polymeric film used in the simulations. For the conventional interdiffusion of solvent-glassy polymers (with long chains entangled together), the expected Case II diffusion is usually characterized by a sharp solvent front which diffuses linearly with time into the polymer. Behind the front, the solvent concentration often is uniform. The creation of sharp front in Case II diffusion can be readily understood from the concentration-dependent diffusion rate of the solvent and the corresponding glass-to-rubber transition

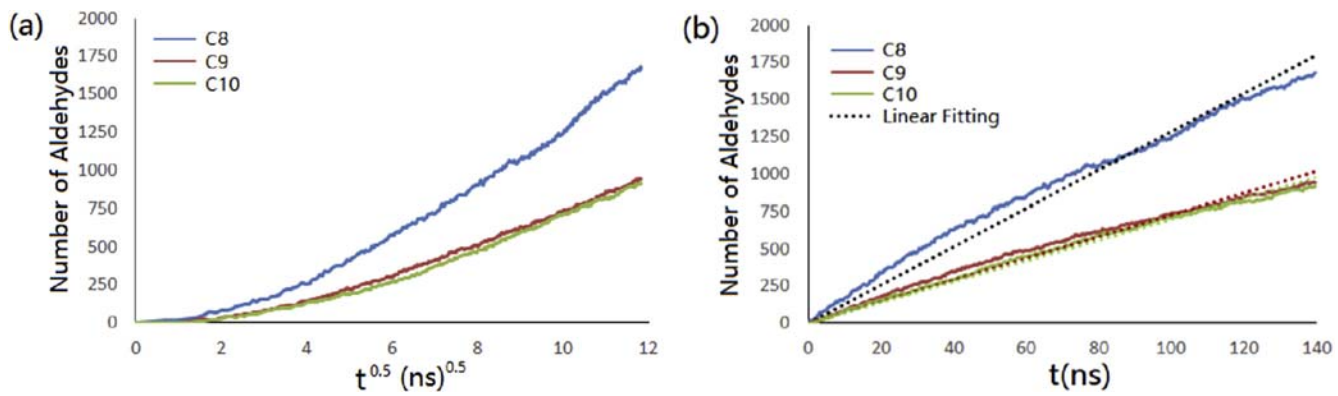

Fig. 8. Mass uptakes of the aldehyde molecules by the polymer film versus (a) $t^{0.5}$, and (b) t at T = 300 K.

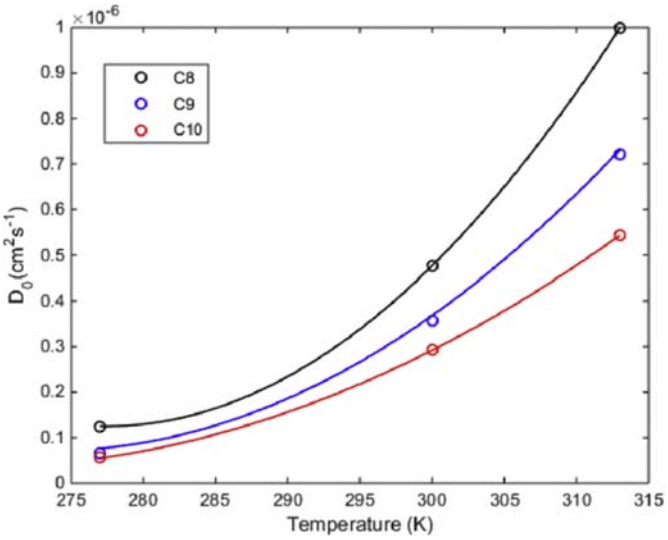

Fig. 10. Temperature dependent diffusivity constants for the three aldehyde systems. Solid curves are the 2-order polynomial fits to the computed values.

in the polymer. That is, there is a point in the polymer film where the critical solvent concentration will induce the glass-to-rubber transition. Diffusion of the solvent ahead of this point (with a rate of "D-glass") is very slow because of the glassy state of the polymer. While behind this point, diffusion of the solvent (with a rate of "D-rubber") is fast. The significant diffusion discrepancy then creates a sharp solvent front in the polymeric film, which propagates at a rate determined by the time-independent viscoelastic relaxation response of the polymer. Consequently, it limits the maximum solvent flux at the front and results in the linear mass uptakes with time. In the "D-glass" region, recent experiments also show that there is a Fickian-type precursor extending to a very short distance ahead of the sharp front [49,50]. Thus, the Fickian-type precursor, the "D-glass" and the "D-rubber" diffusions along with the concentration profile are the three key features of the Case II diffusion. In the first case, when "D-glass" is far less than "D-rubber", the sharp front (with a uniform concentration behind it) is established in a very short time. The solvent flux in the "D-glass" region then dominates the mass uptakes, and the system exhibits an obvious Case II diffusion feature. However, in the second case when "D-glass" is less but close to "D-rubber", it will need much longer time to create the sharp front. Therefore, before the sharp front is established, the solvent flux in the film is determined by the combined effect of "D-glass" and "D-rubber" diffusions. If the "D-rubber" diffusion is dominant in this combined effect, the system will show an approximate Fickian-type diffusion behavior. Otherwise, the Case II diffusion is exhibited. In the current aldehyde-polymer simulations, due to the short polymer chains and the uncured polymeric film (Tg = 315 K) the system belongs to the above-mentioned second case, which can be clearly seen from the plot of D(ρ) in Fig. 7. Therefore, a convex upwards density profile is gradually formed in Fig. 5, and the approximate Fickian-type diffusion is seen in the scaled density profiles in Fig. 6.

The developed CG MD simulation framework for studying the aldehyde-polymer film interdiffusion extends the accessible spatial- and time-scales for the interdiffusion. Based on the extended long-time interdiffusion density profiles, the aldehyde diffusivity constants (D_0 in Eq. (1)) and their dependence on the density/concentration (D(ρ) in Eq. (3)) in the studied glassy polymeric film are found to be $\sim 10^{-7} cm^2 s^{-1}$. However, due to the ambiguous definition of the time-scale in the CG simulations, these do not represent the absolute diffusion rates between those two materials in experiments. They also significantly differ from diffusivities obtained from the all-atom (AA) simulations. Generally, the dynamics in CG simulations is faster than that in the AA simulations because the intermolecular friction forces are much smaller and the corresponding energy landscape is much smoother in the CG model due to the use of larger particle sizes [39] than that in the AA simulations. Therefore, a time scale mapping procedure needs to be developed for accurately predicting the diffusivity of small molecule-polymer interdiffusion from the CG simulation results.

An intuitively obvious technique for developing this time scale mapping $\tau_{CG\rightarrow Exp}(T)$, is by directly comparing the CG diffusivity (D_o^{CG}(T) in Fig.10) with the experimental results ($D_o^{Exp}(T)$) for a few reference systems. Based on the $\tau_{CG\rightarrow Exp}(T)$ data, an empirical model can be developed to quantitatively predict the diffusivity of small molecule-polymer interdiffusion over a range of temperatures. However, due to the lack of $D_o^{Exp}(T)$ data, the indirect time scale mapping derived by comparing the self-diffusion constants in CG (D_S^{CG}) and atomistic (D_S^{AA}) simulations is applied in the current work as has been done by other researchers [18,39,51,52]. It is based on the assumption that the atomistic simulations, within error bars, follow the experimental data. This has been validated for the self-diffusion constants of the molten polymer matrices [21,22,53].

The C8 aldehydes diffusion in the current uncross-linked polymer matrix is tested as the benchmark example to calculate the concentration- and the temperature-dependent time mapping factor ($\tau_{CG\rightarrow AA}(c,T) = D_S^{CG}/D_S^{AA}$). By using the C8-polymer mixture CG and atomistic models [40], the C8 self-diffusion constants (D_S^{CG} and D_S^{AA}) are computed from their linear parts of the MSDs vs. time curves and employing the Einstein relation. We have simulated the diffusion of 20, 30, 60, 90 and 120 C8 aldehydes molecules into the polymer matrix for the temperature varying from 300 K to 360 K [40] (see Appendix B). These results show that within the studied concentration and temperature ranges, the time mapping factors $\tau_{CG\rightarrow AA}(c,T)$ vary between 2 and 3. Thus dividing the presently computed diffusivities (D_0 in Eq. (1) and D(ρ) in Eq. (3)) by the relatively constant $\tau_{CG\rightarrow AA}$ factor, preliminary estimates of the dynamics of the C8-polymer interdiffusion can be found. Though $\tau_{CG\rightarrow AA}$ is determined from the self-diffusion constants, it is noted that in the dilute limit (ρ→0), the diffusivity D(ρ) is theoretically equal to the self-diffusion constant $D_s^{CG}(\rho)$. Indeed, as shown in Fig. 7, D(ρ→0) for the C8 aldehydes is about $0.783 \times 10^{-7} cm^2 s^{-1}$, which is very close to $D_s^{CG} = 0.589 \times 10^{-7} cm^2 s^{-1}$ for the diffusion of the 20 C8 aldehyde molecules into the polymer matrix.

Besides the ambiguity in the time scale, the accurate description of the interdiffusion material systems by the CG model is another important factor that affects the diffusivity prediction. In current simulations, the CG polymer film has been modeled without considering cross-linking. The cross-linking will reduce relaxation rates of the polymer segments in the film. Thus, it is expected that the presently calculated diffusivities would be higher than their absolute values, even after correcting for the time scale. Therefore, they can only be treated as an upper bound for the dynamics of the aldehyde-polymer interdiffusions. A cross-linked polymer film model should be developed to improve upon the accuracy of the diffusivity prediction.

5. Conclusions

We have used coarse-grained (CG) molecular dynamics (MD) simulations to study the interdiffusion of small aldehyde molecules into a polymer film composed of four constituents. Effects of the penetrator molecule size, water and temperature on the interdiffusion processes have been probed in detail. The following conclusions are drawn from the results presented above.

(1) For the studied C8, C9 and C10 aldehydes, the interdiffusion processes with the polymeric film generally follow *the smaller-the faster* rule. The C8 aldehydes described by two CG beads with the smallest molecule size interdiffuse fastest into the polymer film, while the C9 and the C10 aldehydes represented by the three CG beads interdiffuse slower than the C8 molecules but essentially at the same rate because of their similar non-bonded interactions with the polymer film. This indicates that the developed CG models capture well the size effect of the aldehyde-polymer interdiffusion.

(2) Water molecules significantly affect the adsorption and the initial interdiffusion of the aldehyde molecules onto/into the polymer film. Before the aldehydes adsorption, phase separation between the aldehyde and the water molecules is observed which is due to the low solubility of the aldehydes in water. After the aldehydes adsorption, a three layer sandwich interdiffusion structure (water-aldehyde-polymer) is formed. The interdiffusion occurs only between the adsorbed aldehyde layer and the polymeric film. Water molecules only affect the initial aldehyde-polymer interdiffusion, and play a negligible role once the aldehyde molecules have diffused deep into the film.

(3) Asymmetric interdiffusions are found in the three aldehyde systems studied. On the polymer-rich side of the interface, the Fickian precursor diffusion dominates the interdiffusion processes as evidenced by scaling of the density profiles with $t^{0.5}$. On the aldehyde-rich side, the interdiffusion deviates from the Fickian diffusion due to swelling of the polymeric film.

(4) Aldehyde diffusivities into the polymer film are highly concentration dependent. They exhibit a ballistic increase at low concentration and an exponential increase at high concentration. As a first approximation, Fick's second law with a constant diffusivity can well fit the density profiles in the polymer-rich region, though the diffusion mechanism is expected to be case II diffusion with Fickian precursors.

(5) Aldehydes diffusivities are also strongly temperature dependent, and increase with an increase in the temperature. The C8 aldehyde diffusivities have a higher temperature sensitivity than the C9 and the C10 aldehydes.

(6) The CG simulations can only predict the relative, rather than the absolute, values of the aldehyde diffusivity. These values can be refined by using a cross-linked polymer film model in the simulations and deducing the time scale by correlating the experimental and the computed values for a representative set of samples.

Appendix A

Table A1
CG parameters of bonded interactions for the aldehyde-polymer film systems.

Polymer component	Bond	r_0(nm)	K_b ($kJmol^{-1}nm^{-2}$)	Angle	θ_0(deg)	K_a ($kJmol^{-1}$)
PMA	M1-M1	0.24	12,700	M1-M1-M1	180	4.15
	M1-M2	0.27	21,100	M1-M1-M2	100	4.32
				M2-M1-M1	80	10.83
EAA	E1-E1	0.257	38,500	E1-E1-E1	180	12.50
	E1-E2	0.235	51,300	E1-E1-E2	110	21.705
				E2-E1-E1	75	38.022
LPEI	L1-L1	0.355	2600	L1-L1-L1	180	9.57
BPEI	B1-B2	0.31	17,100	1-2-3	110	673.57
	B1-B3	0.37	27,100	2-3-4	110	305.38
	B2-B3	0.312	33,800	3-4-5	110	204.96
	B3-B3	0.385	16,300	8-7-3	120	100.78
				6-1-2	40	9.98
				10-9-4	70	8.73
				11-9-4	160	12.50
				10-9-11	40	167.73
				3-4-9	140	100.78
				5-4-9	40	4.55
				2-3-7	120	12.50
				4-3-7	80	16,684
C8	O1-O2	0.47	1250			
C9	O3-O3	0.375	8575	O3-O3-O2	180	25.0
	O3-O2	0.415	1210			
C10	O3-O1	0.425	5645	O3-O1-O2	180	20.87
	O1-O2	0.405	1250			

Table A2
CG parameters of non-bonded interactions for the aldehyde-water-polymer film systems (σ-nm/ε-$kJmol^{-1}$).

	SC2	SP3	Na	SNd	SNa	Nd	C1	C2	P1	P4	Wall
SC2	0.43(2.625)	0.43(2.0)	0.47(2.70)	0.43(2.0)	0.43(2.0)	0.47(2.70)	0.47(3.50)	0.47(3.50)	0.47(3.0)	0.47(2.30)	0.47(0.01)
SP3		0.43(3.75)	0.47(4.50)	0.43(3.375)	0.43(3.375)	0.47(4.50)	0.47(2.30)	0.47(2.70)	0.47(4.50)	0.47(5.0)	0.47(0.01)
Na			0.47(4.0)	0.47(4.50)	0.47(4.0)	0.47(4.50)	0.47(2.70)	0.47(2.70)	0.47(4.50)	0.47(4.0)	0.47(0.01)
SNd				0.43(3.0)	0.43(3.375)	0.47(4.0)	0.47(2.70)	0.47(2.70)	0.47(4.50)	0.47(4.0)	0.47(0.01)
SNa					0.43(3.0)	0.47(4.50)	0.47(2.70)	0.47(2.70)	0.47(4.50)	0.47(4.0)	0.47(0.01)
Nd						0.47(4.0)	0.47(2.70)	0.47(2.70)	0.47(4.50)	0.47(4.0)	0.47(0.01)
C1							0.47(3.50)	0.47(3.50)	0.47(2.70)	0.47(2.0)	0.47(0.01)
C2								0.47(3.50)	0.47(3.10)	0.47(2.30)	0.47(0.01)
P1									0.47(4.50)	0.47(4.50)	0.47(0.01)
P4										0.47(5.0)	0.47(0.01)
Wall											0.0 (0.0)

Appendix B

Table B1
Concentration-dependent time mapping factor for the C8 aldehydes at T = 300 K.

Number of C8	Atomistic density $\rho^{AA}(gcm^{-3})$	Self-diffusion rate $D_s^{AA}(\times 10^{-11} m^2 s^{-1})$	CG density $\rho^{CG}(gcm^{-3})$	Self-diffusion rate $D_s^{CG}(\times 10^{-11} m^2 s^{-1})$	Scaling factor D_s^{CG}/D_s^{AA}
20	0.925 ± 0.005	0.203	0.937 ± 0.004	0.589	2.901
30	0.925 ± 0.005	0.398	0.937 ± 0.005	0.983	2.470
60	0.922 ± 0.006	0.452	0.940 ± 0.004	1.498	3.313
90	0.920 ± 0.005	0.621	0.943 ± 0.004	1.896	3.053
120	0.918 ± 0.005	0.943	0.945 ± 0.005	1.989	2.089

Table B2
Temperature-dependent time mapping factor for 20 C8 aldehyde molecules diffusing into the polymer.

T (K)	Atomistic density $\rho^{AA}(gcm^{-3})$	Self-diffusion rate $D_s^{AA}(\times 10^{-11} m^2 s^{-1})$	CG density $\rho^{CG}(gcm^{-3})$	Self-diffusion rate $D_s^{CG}(\times 10^{-11} m^2 s^{-1})$	Scaling factorD_s^{CG}/D_s^{AA}
300	0.925 ± 0.005	0.203	0.937 ± 0.004	0.589	2.901
320	0.917 ± 0.008	0.725	0.930 ± 0.005	1.786	2.461
330	0.902 ± 0.010	1.220	0.929 ± 0.006	3.337	2.734
340	0.905 ± 0.010	2.642	0.929 ± 0.006	6.201	2.347
350	0.899 ± 0.012	3.076	0.923 ± 0.008	6.630	2.156
360	0.891 ± 0.012	4.952	0.921 ± 0.008	12.37	2.569

References

[1] O.Y. Kwapong, J.H. Hotchkiss, J. Food Sci. 52 (3) (1987) 761–763.
[2] V. Ducruet, O. Vitrac, P. Saillard, E. Guichard, A. Feigenbaum, N. Fournier, Food Addit. Contam. 24 (11) (2007) 1306–1317.
[3] S.G. Charati, S.A. Stern, Macromolecules 31 (16) (1998) 5529–5535.
[4] S.Y. Lim, M. Sahimi, T.T. Tsotsis, N. Kim, Phys. Rev. E 76 (1) (2007) 011810.
[5] D. Jenke, Late Stage Product Development. Compatibility of Pharmaceutical Products and Contact Materials, John Wiley & Sons, Inc, 2008, pp. 229–247.
[6] J.S. Edward, T.P. Eugene, Elastomeric Components for the Pharmaceutical Industry. Encyclopedia of Pharmaceutical Science and Technology, fourth ed., CRC Press, 2013, pp. 1330–1351.
[7] S.B. Kulkarni, M.Y. Kariduraganavar, T.M. Aminabhavi, J. Appl. Polym. Sci. 89 (12) (2003) 3201–3209.
[8] D. Cava, J.M. Lagarón, A. López-Rubio, R. Catalá, R. Gavara, Polym. Test. 23 (5) (2004) 551–557.
[9] M. Moaddeb, W.J. Koros, J. Appl. Polym. Sci. 57 (6) (1995) 687–703.
[10] J.S. Vrentas, C.M. Vrentas, Eur. Polym. J. 34 (5–6) (1998) 797–803.
[11] E. von Meerwall, S. Beckman, J. Jang, W.L. Mattice, J. Chem. Phys. 108 (10) (1998) 4299–4304.
[12] K. Ganesh, R. Nagarajan, J.L. Duda, Industrial Eng. Chem. Res. 31 (3) (1992) 746–755.
[13] I. Cozmuta, M. Blanco, W.A. Goddard, J. Phys. Chem. B 111 (12) (2007) 3151–3166.
[14] M.L. Greenfield, D.N. Theodorou, Macromolecules 34 (24) (2001) 8541–8553.
[15] D. Pavel, R. Shanks, Polymer 46 (16) (2005) 6135–6147.
[16] S. Neyertz, A. Douanne, D. Brown, J. Membr. Sci. 280 (1–2) (2006) 517–529.
[17] H. Kikuchi, S. Kuwajima, M. Fukuda, Chem. Phys. Lett. 358 (5–6) (2002) 466–472.
[18] D. Fritz, C.R. Herbers, K. Kremer, N.F.A. van der Vegt, Soft Matter 5 (22) (2009) 4556–4563.
[19] L.-H. Cai, S. Panyukov, M. Rubinstein, Macromolecules 48 (3) (2015) 847–862.
[20] M. Tsige, G.S. Grest, J. Chem. Phys. 120 (6) (2004) 2989–2995.
[21] G.E. Karlsson, T.S. Johansson, U.W. Gedde, M.S. Hedenqvist, Macromolecules 35 (19) (2002) 7453–7459.
[22] A. Mattozzi, M.S. Hedenqvist, U.W. Gedde, Polymer 48 (17) (2007) 5174–5180.
[23] Z.-W. Wang, P.-L. Wang, C.-Y. Hu, Packag. Technol. Sci. 23 (8) (2010) 457–469.
[24] M. Tsige, G.S. Grest, J. Chem. Phys. 121 (15) (2004) 7513–7519.
[25] F. Pierce, D. Perahia, G.S. Grest, Macromolecules 42 (20) (2009) 7969–7973.
[26] J. Zeng, A. Wang, X. Gong, J. Chen, S. Chen, F. Xue, Chin. J. Chem. 30 (1) (2012) 115–120.
[27] V.A. Harmandaris, N.P. Adhikari, N.F.A. van der Vegt, K. Kremer, B.A. Mann, R. Voelkel, H. Weiss, C. Liew, Macromolecules 40 (19) (2007) 7026–7035.
[28] A. Gautieri, S. Vesentini, A. Redaelli, J. Mol. Model. 16 (12) (2010) 1845–1851.
[29] A.A. Gusev, U.W. Suter, J. Chem. Phys. 99 (3) (1993) 2228–2234.
[30] M.L. Greenfield, D.N. Theodorou, Macromolecules 31 (20) (1998) 7068–7090.
[31] J. Han, R.H. Boyd, Macromolecules 27 (19) (1994) 5365–5370.
[32] T.R. Cuthbert, N.J. Wagner, M.E. Paulaitis, G. Murgia, B. D'Aguanno, Macromolecules 32 (15) (1999) 5017–5028.
[33] M. Fukuda, S. Kuwajima, J. Chem. Phys. 108 (7) (1998) 3001–3009.
[34] R.H. Boyd, P.V.K. Pant, Macromolecules 24 (23) (1991) 6325–6331.
[35] F. Mueller-Plathe, S.C. Rogers, W.F. Van Gunsteren, Macromolecules 25 (24) (1992) 6722–6724.
[36] N.E. Schlotter, P.Y. Furlan, Polymer 33 (16) (1992) 3323–3342.
[37] A. Peychès-Bach, M. Moutounet, S. Peyron, P. Chalier, J. Food Eng. 95 (1) (2009) 45–53.
[38] S. Aucejo, M.J. Pozo, R. Gavara, J. Appl. Polym. Sci. 70 (1998) 711–716.
[39] S.J. Marrink, H.J. Risselada, S. Yefimov, D.P. Tieleman, A.H. de Vries, J. Phys. Chem. B 111 (27) (2007) 7812–7824.
[40] E. Lin, X. You, R.M. Kriegel, R.D. Moffitt, R.C. Batra, Colloids Surf. A Physicochem. Eng. Asp. 522 (2017) 152–160.
[41] H. Yagyu, Y. Hirai, A. Uesugi, Y. Makino, K. Sugano, T. Tsuchiya, O. Tabata, Polymer 53 (21) (2012) 4834–4842.
[42] S. Plimpton, J. Comput. Phys. 117 (1) (1995) 1–19.
[43] L. Enqiang, S. Huiji, N. Lisha, Modelling and simulation in materials science and engineering 22 (3) (2014) 035012.
[44] E.Q. Lin, H.J. Shi, L.S. Niu, E.Z. Jin, Comput. Mater. Sci. 59 (2012) 94–100.
[45] S.H. Yalkowshy, Y. He, P. Jain, Handbook of Aqueous Solubility Data, 2nd ed., CRC Press, Boca Raton, USA, 2010.
[46] S.J. Marrink, A.H. de Vries, A.E. Mark, J. Phys. Chem. B 108 (2) (2004) 750–760.
[47] T. Kubo, T. Nose, Polym. J. 24 (12) (1992) 1351–1361.
[48] S. Yang, J. Qu, Polymer 53 (21) (2012) 4806–4817.
[49] Q.Y. Zhou, A.S. Argon, R.E. Cohen, Polymer 42 (2) (2001) 613–621.
[50] D.F. Stamatialis, M. Sanopoulou, J.H. Petropoulos, Macromolecules 35 (3) (2002) 1021–1027.
[51] G. Rossi, L. Monticelli, S.R. Puisto, I. Vattulainen, T. Ala-Nissila, Soft Matter 7 (2) (2011) 698–708.
[52] S.O. Nielsen, C.F. Lopez, G. Srinivas, M.L. Klein, J. Chem. Phys. 119 (14) (2003) 7043–7049.
[53] V.A. Harmandaris, M. Doxastakis, V.G. Mavrantzas, D.N. Theodorou, J. Chem. Phys. 116 (1) (2002) 436–446.